Scientific Research Publishing

Materials Sciences and Applications, 2022, 13, 401-416
https://www.scirp.org/journal/msa
ISSN Online: 2153-1188
ISSN Print: 2153-117X

Morphological, Biological and Physicochemical Evaluation of ABS-Based Systems Containing Graphene Obtained by 3D Printing via Solution

Antônio Carlos Santos Thiele*, Maria Inês Bruno Tavares

Instituto de Macromoléculas Professora Eloisa Mano (IMA), Universidade Federal do Rio de Janeiro, Rio de Janeiro, RJ, Brazil
Email: *antoniothiele@ima.ufrj.br

How to cite this paper: Thiele, A.C.S. and Tavares, M.I.B. (2022) Morphological, Biological and Physicochemical Evaluation of ABS-Based Systems Containing Graphene Obtained by 3D Printing via Solution. *Materials Sciences and Applications*, **13**, 401-416.
https://doi.org/10.4236/msa.2022.136023

Received: February 19, 2022
Accepted: June 26, 2022
Published: June 29, 2022

Abstract

3D printing is a valuable resource that allows flexibility in the production of objects based on a virtual file. When it is combined with nanotechnology, new features can be added to existing materials. Thus, form and function can be associated to achieve a specific goal, such as the development of support structures for cell growth applicable to systems aiding tissue regeneration. Based on this rationale, the present work proposes a system composed of ABS and graphene nanoparticles solubilized in acetone to be 3D impressed using solvent casting technique. Our main goal was to develop a biocompatible and non-degradable material that fully makes use of the design versatility of 3D printing, to enable new practical employments in the future, for example in the medical field. In this study, different characterization techniques were used—such as microscopy, TGA, DSC, and others—to understand the features and properties of the material obtained, as well as the viability of its use and diffusion. Moreover, the artifacts impressed proved to be non-cytotoxic and promoted cellular adhesion to the cellular lineage of fibroblasts L929. In sum, we believe that the technology described in this article has the potential to serve as a basis for the development of future biocompatible materials that take advantage of their three-dimensional design to perform their functions.

Keywords

Acrylonitrile Butadiene Styrene, Graphene Nanoplatelets, 3D Printing, Biocompatibility

1. Introduction

3D printing consists of a group of technologies able to produce artifacts based on

virtual models through overlapping layers of materials [1]. This process allows the production of geometries that were considered complex for traditional production methods. In other words, 3D printing has the great advantage to allow remarkable versatility and wide customization of artifacts to be produced.

However, it is necessary to point out that 3D printing is not a homogeneous field. In fact, it refers to a variety of different technologies. Among the 3D printing technologies available, the most found is fused filament fabrication (FFF). That process builds artifacts by successively depositing layers of molten thermoplastic that solidifies after cooling [2]. Despite its innovative nature, FFF suffers from a crucial vulnerability. It is complicated to incorporate charges in the material with this technique, once it must be done through an extrusion process to produce filaments. For this reason, it is dependable of filaments available on the market.

To fix this problem, many studies have used a FFF derivation technic called direct deposition or 3D plotting (DP). In DP, layers of viscous polymer solutions are deposited. The machinery for this technique is the same used for FFF, except for the print head, which is replaced by a fluid extruder. Different from FFF, DP is the most versatile technique, able to use pasty material, and its system can be pneumatic, compressed air, piston motion or screw rotation [3] [4]. When the solutions employed in DP are formed of a volatile solvent, the technique is called solvent casting 3D printing. The biggest advantage of this process is that once the solvent leaves and evaporates, the material hardens. Therefore, solvent casting technique enables the incorporation of nanoparticles in 3D printing, and allows its use in many fields, such as development of conducting materials, creation of shields to electromagnetic fields, etc [3] [5] [6].

The incorporation of charges into 3D printing processes is a relevant issue to many studies. In general, charges are commonly incorporated to widen the functionalities of plastic materials. For example, graphene nanoparticles in the polymeric matrix provide new specific characteristics to desired applications, such as more resistance or better biocompatibility [7] [8].

In tune with the main works in the field, the present study proposes a biocompatible non-degradable system composed of nanoparticles of lamellar graphene dispersed in an ABS matrix intended to be loaded as a solvent casting 3D print material.

This polymeric solution derives from the ones traditionally presented in the related literature. Firstly, studies commonly apply a pair of solvents, such as dimetilformamida (DMF) and acetone, or only dichloromethane (DCM). In this research, we decided to use only acetone, the less toxic among the three solvents. Secondly, while the literature generally applies PLC and PVDF, we preferred to use ABS, even though it is not biodegradable, it shows high mechanical resistance. Besides that, the option for ABS is justified for the fact that it presents cellular adhesion, as the literature has already shown [9]. It is relevant to mention that for biological applications ABS M30i must be used [10]. Thirdly, we

incorporate graphene nanoparticles in the solution to potentialize the biocompatibility and cellular adhesion in the polymeric matrix chosen.

Finally, this work was motivated by the search of a new composite to be impressed in solvent casting 3D printing that could have wider applications. We truly expect that the technology described here also encourages further studies and applications, such as in the medical field.

2. Materials and Methods

2.1. Materials

- ABS: The ABS acquired was from the NatureWorks brand in pellet form;
- Graphene was purchased from XG Sciences, Michigan, and United States of America. Graphene nanoplatelets (GnP-5), M grid, average particle diameters of 5 μm, thickness approximately 6 nm, typical surface area between 120 - 150 m^2/g and density 2.2 g/cm^3;
- Acetone 99% purity supplied by Acetone and ethanol P.A. from ISOFAR.

2.2. Methods for Obtaining Nanocomposites

The systems were obtained via solution using acetone as solvent [3]. For the development of the systems, a concentration of 30% of polymer m/m in relation to the solvent mass was used. The high polymer concentration is necessary so that the structure of the piece is maintained after printing, without its collapse occurring before the solvent exits [5] [11]. The nanoparticles, in turn, were varied in concentrations of 0.01%, 0.05% and 0.1% m/m in relation to the ABS mass used in the systems. The composition of the systems and the nomenclature of each group are described in Table 1.

To obtain the systems, the particles were initially dispersed in acetone through sonication in a tip sonicator (Ultronique, model: QR500), using 50% of its power in two cycles of 2 minutes. The short dispersion cycles aimed to limit the increase in the temperature of the medium caused by sonication so that there were no significant losses of solvent volume by volatilization. After dispersing the particles, ABS in pellet form was added to the systems and the system was kept under magnetic stirring for 3 hours at room temperature until complete solubilization of the polymer matrix.

After obtaining the ABS/nanoparticle systems in acetone solution, they were printed using 3D solution printing. To this end, a 3D printer was built from a 3D

Table 1. Systems composition and adopted nomenclature.

Systems composition	Adopted nomenclature
ABS pure	ABS-GNP 0%
ABS + graphene nano particle 0.01%	ABS-GNP 0.01%
ABS + graphene nano particle 0.05%	ABS-GNP 0.05%
ABS + graphene nano particle 0.1%	ABS-GNP 0.1%

Graber I3 assembly kit (GTMax) of cast filament, which had its original extruder replaced by a syringe pump. A syringe pump, customized by the author of this article, was used, based on the open-source project of the Ameloot group from the Belgian University of Leuven [12]. In this apparatus, a 30 mL syringe equipped with a needle with a straight end section and an internal diameter of 0.45 mm was attached.

In order to improve the accuracy of the table height calibration and facilitate its setup process, the syringe was used as a calibration probe. The Z-axis ends top was replaced with copper electrodes connected to the negative pole of the reader while the positive pole was connected to the needle, so that calibration is established when the syringe hits the table at each of its 4 corners.

The printing parameters were as follows: layer height = 0.05 mm, infill = 25% rectilinear pattern, fume hood ventilation, no heated table, print speed between 600 mm/min and 1000 mm/min, 20 layers tall. The flow rate of the syringe pump was set at 0.001 ml/s.

Two specimens were drawn: a rectangular measuring 1 cm × 3 cm for mechanical tests and a square with 1 cm side for the other characterizations, both of them can be seen in Figure 1 and Figure 2.

According to previous studies done by the author, it is important to set an interval between printing the layers to allow time for part of the solvent to evaporate. If the material is too soft, it is pulled off the table with the passage of the syringe. To satisfy this condition, 20 specimens were printed simultaneously, which

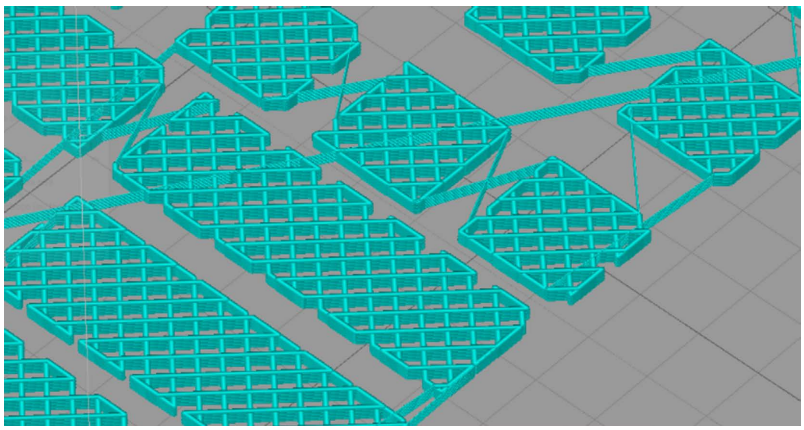

Figure 1. Graphic representation of artifacts in Simplify slicing software.

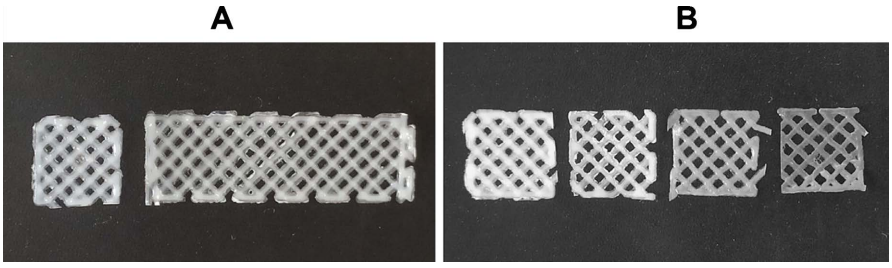

Figure 2. (A) Pure ABS artifacts. 1 cm × 1 cm and 3 cm × 1 cm specimens. (B) From left to right, artifacts with graphene concentration of 0%, 0.01%, 0.05% and 0.1%.

increased the time between layers.

2.3. Characterization Methods

2.3.1. Fourier Transform Infrared Analysis (FTIR)

FTIR analyzes were carried out in order to establish the particle/polymer matrix interaction and evaluate the solvent output of the systems. Analysis were performed at a room temperature of 25˚C in a Perkin Elmer Spectrum version 10.4.2 device and a Frontier FT-IR/FIR model in the ATR function in the observation range from 400 to 4000 cm^{-1}. 60 scans were performed for each sample.

2.3.2. Optical Microscopy

Optical microscopy aimed to evaluate the structure of the material obtained and observe the possible aggregates of particles that could be found in its analysis scale. Micrographs were obtained using an Olympus BX50 optical microscope equipped with a Figure capture camera using a magnification of 100 μm and a room temperature of 21˚C.

2.3.3. Scanning Electron Microscopy

It was used to determine the printed structure by evaluating the precision generated in the printing process and its surface smoothness. Analyses were performed in a JEOL model JSM-5610LV device using a magnification of 100 μm.

2.3.4. Nuclear Magnetic Resonance (NMR)

The NMR analysis was used in order to observe the presence of regions with different mobility in the material. The equipment used was MARAN Ultra 0.54 T (23.4 MHz for 1H), probe diameter: 18 mm and Point Adjustment software: WinDXP 1.8.1 and Originlab OriginPro 8.5.

Analysis were performed with the following specifications: temperature 30˚C ± 2˚C; pulse sequences: inversion—recovery (p180x tau-p90x); pulse duration 90˚ (us): 7.5; logarithmic list of time between pulses (ms): 0.01—10,000; number of Points: 40; number of scans: 4; recycle time (s): 1; receiver gain (dB): 34.

2.3.5. Thermogravimetric Analysis (TGA)

The TGA analysis aimed to evaluate the resistance and thermal degradation of the obtained samples, as well as the solvent output of the samples. Analyses were carried out between 30 and 700˚C in a TGA Q-500 Thermogravimetric device using a heating rate of 10˚C/min and a N_2 atmosphere.

2.3.6. Differential Scanning Calorimetry (DSC)

To determine the thermal parameters of the printed samples, DSC analysis were done on the TA-Instruments Q.1000 differential scanning calorimeter with a heating rate of 10˚C/min in the range of 0˚C to 250˚C under N_2 flow of 50 ml/min.

2.3.7. Cell Viability of the L929 Fibroblast Lineage

The study of the cytotoxicity of the systems was carried out in a L929 cell line

(provided from Rio de Janeiro Cell Bank—BCRJ) following the methodology of Narayanamurthy *et al.* [13] and the standards of ISO 10993-5 [14]. To this end, we used fibroblasts from the L929 cell line that were cultivated in essential medium supplemented with gentamicin and glutamine in a controlled environment at 37˚C and 5% CO_2.

Three samples from each system were initially conditioned in distilled water at 37˚C for 24 hours and then sterilized using exposure of the materials to ethylene gas for 4 hours. After this step, the samples were conditioned in cell culture plates in contact with aliquots of the cell culture medium obtained, remaining an aliquot without contact with the systems to serve as a standard for this analysis. Culture medium was evaluated and replaced every 24 hours for a total of seven days. Cell viability analysis was done using the red dye absorption technique.

For the analysis of neutral red dye, 100 μL of a 0.01% neutral red solution (Sigma Aldrich) was added to each culture plate. After addition of dye, the media were incubated for 3 hours for dye penetration into viable cells. The neutral red dye absorption was then determined by measuring the optical density (OD) in a spectrophotometer (BioTek, Winooski, Vermont, USA) at a wavelength of 492 nm. After analysis, optical density data were compared with the standard (sample without contact with the materials evaluated) in order to estimate the difference in cell viability in the media as a percentage (considering the standard cells as 100% viable).

2.3.8. Cell Adhesion on the Surface of Materials

To carry out the cell adhesion assay, using L929 lineage cells, a culture medium and sample preparation were obtained in a similar way to the one performed for the cytotoxicity assay. After this step, three samples from each system were conditioned in cell culture plates in contact with the obtained cell culture medium. The culture medium was evaluated and substituted every 24 hours for a total of ten days. After this time, the samples were removed from the culture medium and gently washed with water to remove non-adhered cells. After washing the surfaces, the samples were inserted in standardized volumes of essential medium and taken to a Vortex-type shaker (Vortex KASVIbasic K45-2810) at 1000 rpm for 1 minute to remove cells adhered to the surface of the specimens.

The neutral red dye was then added to this medium in a proportion of 300 μL of a 0.01% solution. These media were then analyzed for optical density (OD) at a wavelength of 492 nm using the red dye absorption technique. For the comparison parameter, the total absorbance at 492 nm found in each system was taken into account, which is directly proportional to the number of living cells adhered to the systems [15].

3. Results and Discussion

3.1. Fourier Transform Infrared Analysis (FTIR)

Figure 3 shows the FTIR spectra for the pure ABS artifact and those containing the different concentrations of nanoparticles. The curve for pure ABS proves its

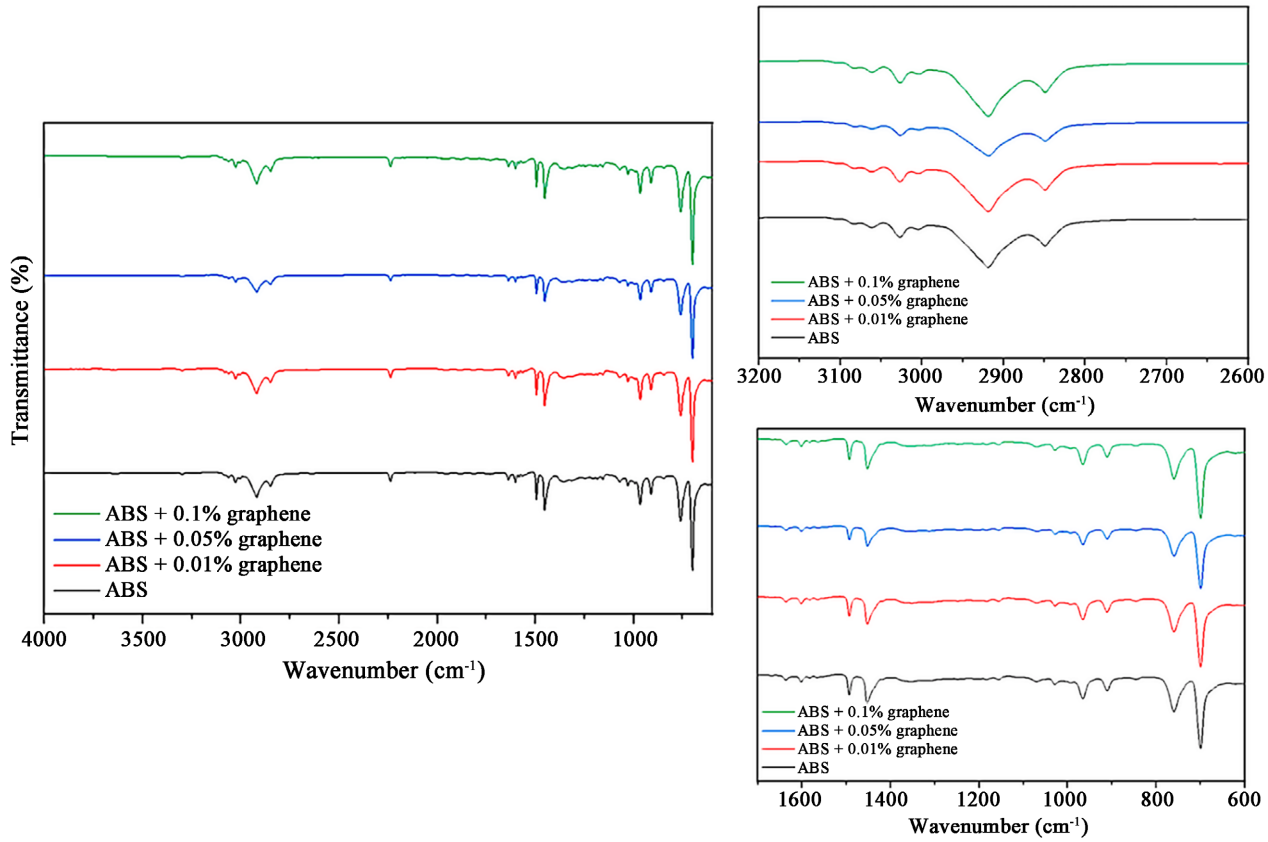

Figure 3. (A) Infrared spectra of the samples. (B) Region expanded between 3200 - 2600 cm^{-1}. (C) Region expanded between 1500 - 600 cm^{-1}.

standard structure and confirmed the FTIR profiles commonly found in the literature for this matrix: in the regions between 3200 - 3000 cm^{-1} and 3000 - 2800 cm^{-1} are, respectively, the connections (-CH-) aromatic and aliphatic; at 2237 cm^{-1} is acrylonitrile (C≡N); between 810 and 690 cm^{-1} is the aromatic ring of styrene; and, finally, between 1130 and 980 cm^{-1} are the bonds (-C=C-) of butadiene [16] [17].

Based on the typical acetone spectrum, there are strong intensity bands at 1230 cm^{-1}, 1358 cm^{-1} and 1710 cm^{-1} which do not overlap the ABS spectrum bands. Thus, the non-observation of these bands in the samples obtained indicates that there are no traces of solvent in percentages large enough to be detected in the sample by the sensitivity of the FTIR technique, suggesting the total removal of solvent from these materials, which will also be evaluated by the TGA [18].

Furthermore, there is no appearance of new bands through the incorporation of nanoparticles, as well as no changes regarding the shape and positioning of the bands in relation to pure ABS, indicating that there is no physical or chemical interaction between the particle and the material that be strong enough to be captured by the FTIR technique.

In the range from 3100 cm^{-1} to 2.600 cm^{-1} is related to the CH_2 and CH_3 axial vibration of polymer, as can better see in the right up. The second important

range is from 1700 cm^{-1} to 600 cm^{-1} that is associated to aromatic and double polymer chains angular vibration. This can see in the right bottom. This result was already expected, since there are no groups likely to interact between the matrix and the particles, which may disfavor an adequate dispersion of the particle in the matrix, as these will tend more strongly to establish particle-particle interactions instead of interactions particle-polymer.

3.2. Optical Microscopy (OM)

In Figure 4 item A and B, it is possible to see structures with a hair-like design in some points of the artifacts. These designs are present in the samples without doping item A and with 0.01% nanoparticles, item B. They are probably caused by the path opened by the solvent at its exit. This accumulation of solvent promoted a separation of the polymer chains, carrying particles which have a greater affinity to the solvent compared to the matrix, creating agglomerates. Another hypothesis is that these designs are formed by roughness or folds on the material surface caused by the contraction of the artifact with the exit of the solvent.

In the ABS-GNP 0.05% and ABS-GNP 0.1% samples, displayed in Figure 5, it is possible to check that the graphene has agglomerated, but it remained well dispersed. This behavior has already been observed in polypropylene and graphene systems [19]. The designs seen in the previous samples have also disappeared.

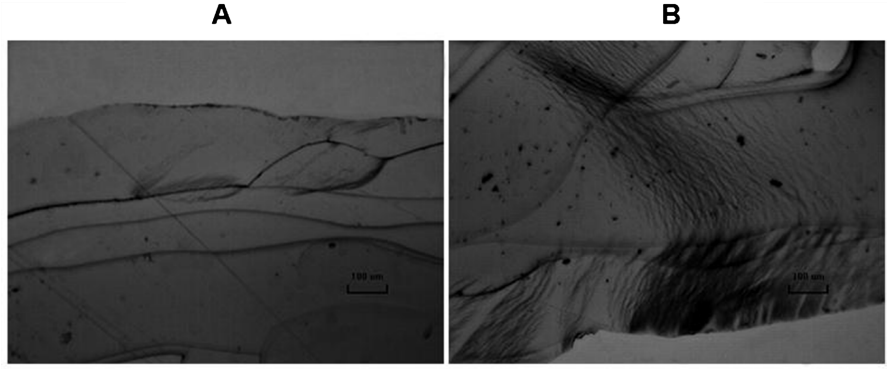

Figure 4. Optical microscopy, 100 μm magnification. (A) Pure ABS sample. (B) Sample ABS-GNP 0.01%.

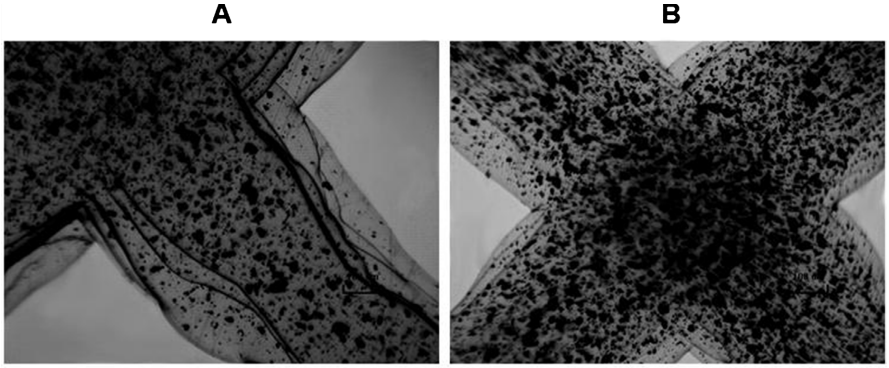

Figure 5. Optical microscopy, 100 μm magnification. (A) Sample ABS-GNP 0.05%. (B) Sample of ABS-GNP 0.1%.

Possibly the agglomerates served as a favoring way for the exit of the solvent.

Figure J software was used to account for and measure the area of the graphene aggregates. In Figure 5 item **A**, 844 aggregates were found, with the area of the smallest and the largest, respectively, 0.2873 μm^2 and 916 μm^2. In Figure 5 item **B**, the aggregate count resulted in a total of 873 clusters. Respectively the areas of the largest and smallest aggregate are 0.2873 μm^2 and 26818 μm^2.

3.3. Scanning Electron Microscopy (SEM)

Scanning electron microscopy, presented at Figure 6, allows us to observe details of the material surface which points high roughness, even at low magnification. This noise is formed by parts of the graphene agglomerates that submerged on the surface of the samples, being a crucial factor for the effectiveness of the system in cell viability and fixation. This is evidenced by Figure 7 item **A** which shows a magnification of one micrometer on the surface of the sample ABS-GNP 0.01%. Figure 7, item **B** shows an enlarged graphene sheet, comparing its geometries it can be said that it is the same material and not a contaminant [7]. To produce this Figure, a small portion of graphene powder was placed on a carbon tape and then a blast of compressed air was applied to remove excess of material.

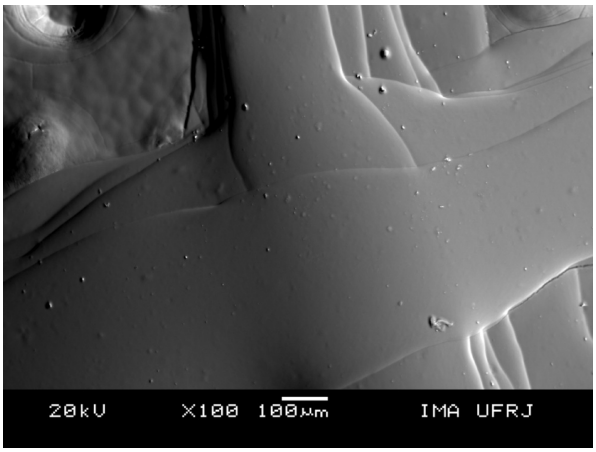

Figure 6. Scanning electron microscopy, 100 μm magnification. Sample ABS-GNP 0.1%.

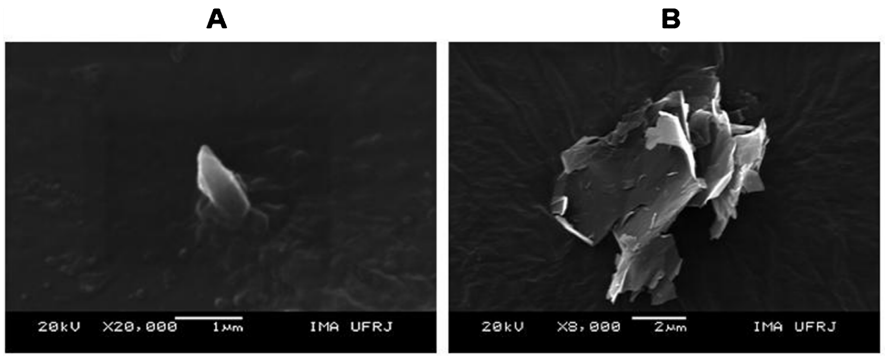

Figure 7. Scanning electron microscopy. (A) Part of a graphene sheet that has been submerged in the material surface, magnification of 1 μm. (B) Agglomerate of graphene sheets, magnification of 2 μm.

Due to the thermal fragility of the material, which will be better addressed in item 3.4, it was not possible to record Figures of the solvent exhaust pores. The rapid degradation of the material prevented magnifications greater than one micrometer.

Figure 6 allows us to see the formation of filaments and irregular layers. The material remains soft for a long time after exiting the syringe and drains to the sides.

The use of more viscous materials with a higher concentration of polymer can improve the resolution, but it is necessary to use printing systems capable of working with high pressure. An alternative would be to choose a more volatile solvent; however they tend to be more toxic.

3.4. Nuclear Magnetic Resonance (NMR)

The addition of graphene hardened the material, causes an increase in the relaxation times (with a constant T_1H) as can see in Figure 8. However, the addition of graphene also caused significant changes in the material structural organization, that is, the form of dispersion of this nanoparticle had a particular or singular action. In ABS-GNP 0.01% system, it is observed that the peak referring to the most rigid region had a narrowing, probably due to a dispersion of this nanoparticle in the matrix. The addition of 0.05% caused a great disorder in the matrix, as the peaks of the two regions with different mobilities increased. And the system ABS-GNP 0.1% generated different organizations in the two domains with different molecular mobilities. This behavior may indicate that the amount of graphene interferes with its distribution in the matrix of this polymer, having greater affinity for the region of greater rigidity.

3.5. Thermogravimetric Analysis (TGA)

Both for pure ABS and for artifacts containing graphene nanoparticles, it is observed

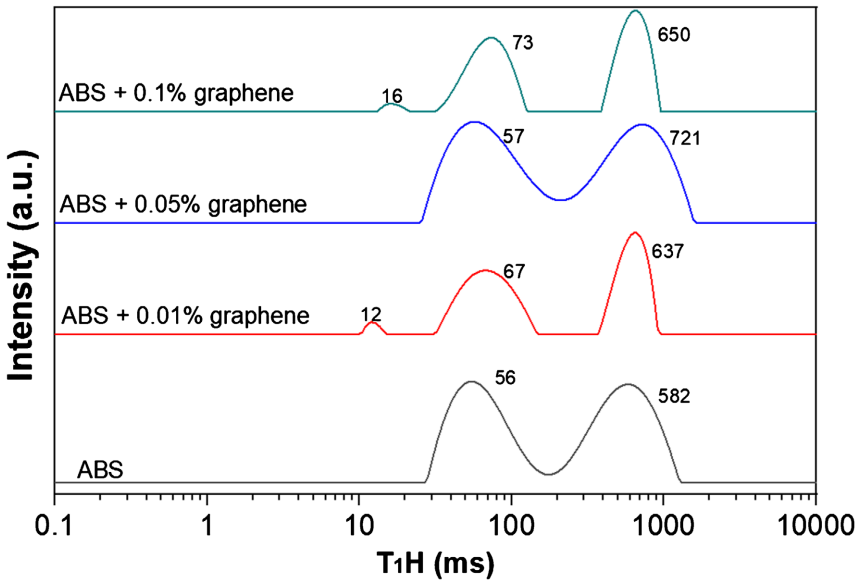

Figure 8. Spin-rede relaxation time measurement.

a very similar thermal degradation profile Table 2.

There is only one material loss event in the normal TGA degradation curve as well as in the DTG derivative, presented at Figure 9. This single-loss profile is common for ABS. As shown in the literature, it describes a range of degradation between 360 and 430, which proves its great thermal stability.

The addition of graphene particles did not cause significant changes in the thermal structure of the material, especially for the load concentrations ABS-GNP 0.05% and ABS-GNP 0.1%. As for ABS-GNP 0.01%, there is a slight decrease in thermal stability. However, taking as a reference their Tpeak and Tonset values, if we extrapolate the equipment's margin of error (±2), we can see that, statistically, this variation is very little significant.

A possible explanation for the decrease in the thermal stability of the system is that the agglomerated graphene has a considerably high thermal conduction capacity. As it is evenly distributed throughout the sample, which is proven by optical microscopy Figures (Figure 5 item **A** and item **B)**, heat is more easily conducted, acting as a degradation accelerator. Added to this, there is the fact that the free volume generated by the graphene agglomerates facilitates the movement of polymer chains, thus promoting the reduction of TG.

Finally, it was not possible to find variation in the amount of waste, even with the addition of graphene due to its low amount, remaining within the equipment error margin.

Table 2. Thermogravimetric values for Tonset, Tpeak and residual for graphene samples 0.01%, 0.05% and 0.1%.

System	T_{onset} (˚C ± 2˚C)	T_{peak} (˚C ± 2˚C)	Residual (%)
Pure ABS 3D	386˚C	410˚C	1%
Graphene 0.01% 3D	381˚C	407˚C	1%
Graphene 0.05% 3D	386˚C	410˚C	1%
Graphene 0.1% 3D	385˚C	409˚C	1%

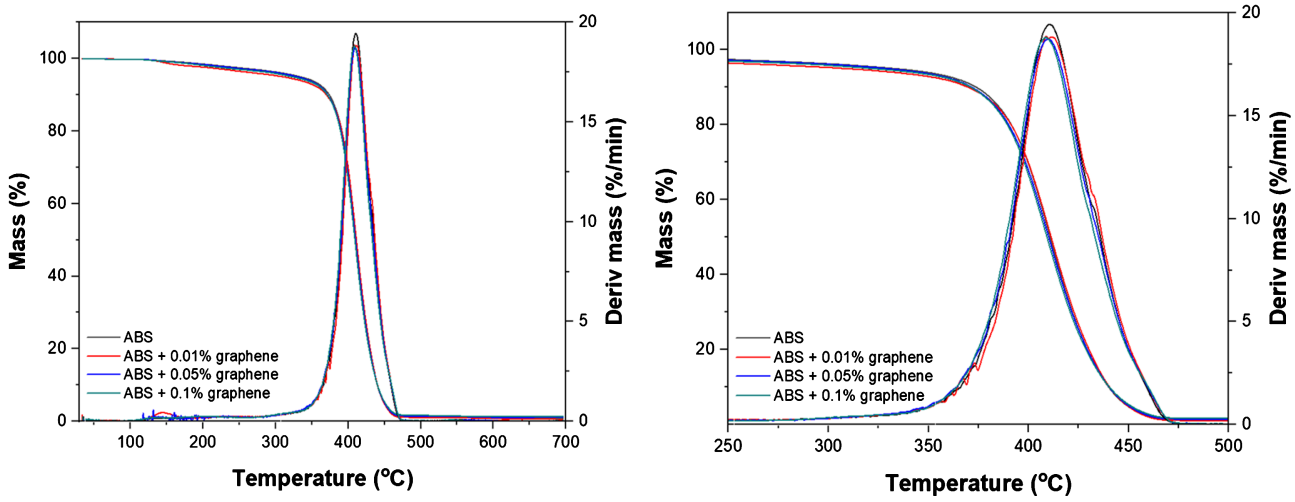

Figure 9. TGA curves of systems representing different graphene contents.

3.6. Differential Scanning Calorimetry (DSC)

Figure 10 exhibits the DSC curves for the systems containing different graphene contents. The pure ABS sample has temperature profiles compatible with those described in the literature. Exhibiting an extended transition composed of two Tg peaks between 110˚C and 135˚C. This is due to more energetic enthalpic relaxation processes linked to segments of the material that are slightly more organized. ABS has a distinct characteristic from conventional amorphous polymers, as it is a block terpolymer.

The addition of particles did not cause significant changes in Tg temperatures. Graphene agglomerates tend to increase the free volume between the chains, causing a reduction in Tg, as they facilitate the relaxation process, but this was not confirmed. Corroborating the hypothesis pointed out in the TGA that there was no significant influence of the increase in free volume in relation to the thermal degradation of the system.

Comparing the curve of the first heating with that of the second, there is a displacement of approximately 3˚C upwards, revealing an impact of the printing technique on thermal transitions. One possible cause for this effect is the stretch caused by shear during wire extrusion.

3.7. Cell Viability of the L929 Fibroblast Lineage

Both pure ABS and GnP-added artifacts have high cell viability, above 90% biocompatibility, which indicates completely non-cytotoxic samples (Figure 11). This behavior is in accordance with the literature [10].

3.8. Cell Adhesion on the Surface of Materials

The cell can be measured through the absorption of a dye by the cells. The greater is this absorption, the greater is the cell adhesion. Analyzing the results, presented in Figure 12, there was an increase in affinity that accompanies the percentage of doping in the systems where the highest adhesion occurs in the

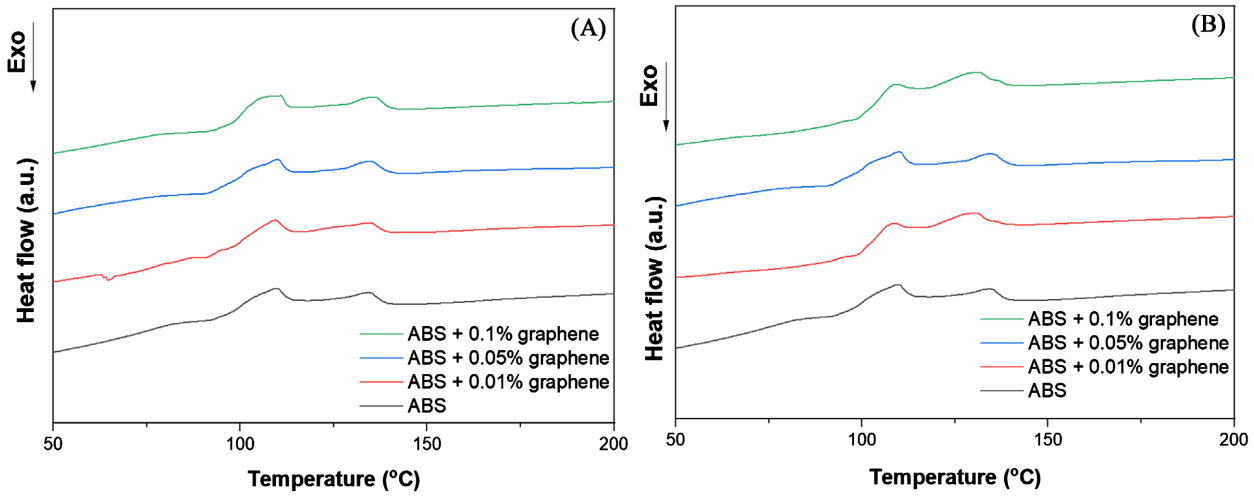

Figure 10. DSC curves of systems representing different graphene contents. (A) first heat. (B) Second heat.

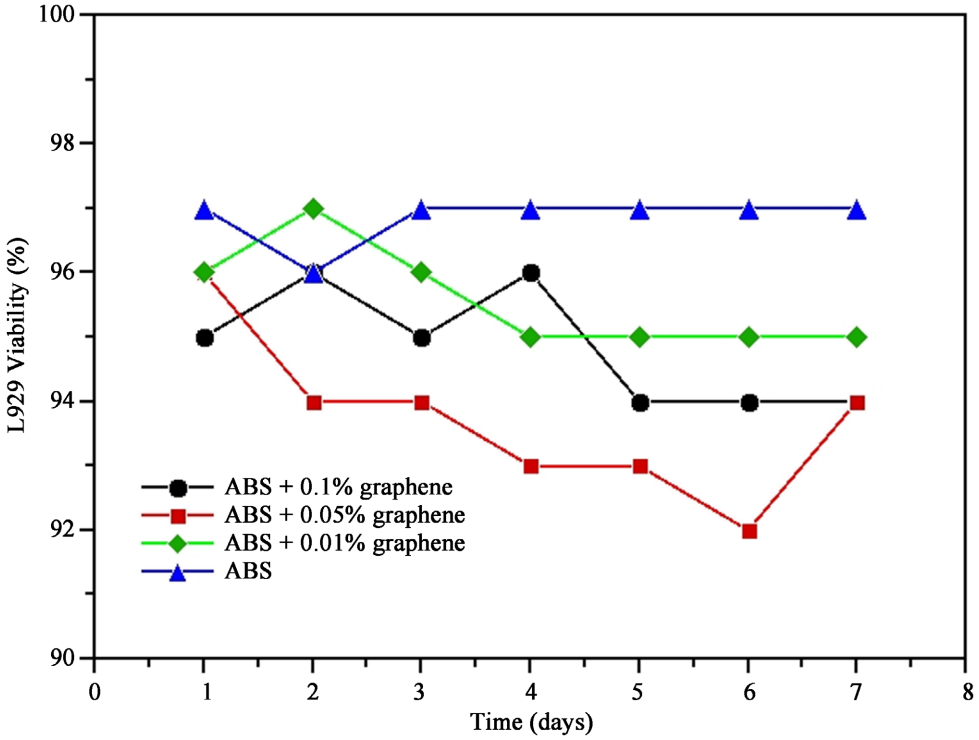

Figure 11. Cell viability of the fibroblast lineage L929 in contact with the systems obtained.

sample with more 0.1% graphene. Studies show a high capacity to promote cell adhesion through graphene, with the supersaturation of the systems; a greater amount of nanoparticles was exposed on the material surface, thus improving cell adhesion as the concentration increases.

Graphene may be acting in three ways to increase cell adhesion. First, by increasing surface wettability, the cells make closer contact with the surface. Second, it increased roughness, which improves cell attachment. Third, the graphene may be generating a piezoelectrical or conductivity condition in the material. Since cell adhesion can be caused by small electrical signals that are interpreted by cells as sodium-potassium modification. A point that corroborates the existence of electrical conduction is the percolation limit. In microscopy it is already possible to see percolation points and there may be contacts between regions of nanometric size. These mechanisms may be acting, but to a lesser extent, due to the insulating nature of the material. Other matrices with an intrinsic piezoelectric nature show better results as PHB, having a piezoelectric nature similar to many organic tissues, such as bones and nervous tissues.

4. Conclusions

Acetone-solubilized ABS/GnP nanocomposites were successfully obtained from the use of tip sonication and mechanical agitation. As a result, specimens were manufactured for the studies using the 3D printing process by solvent casting. With regard to characterizations, the FTIR technique did not indicate a physical or chemical interaction between the particle and the material that is hard enough

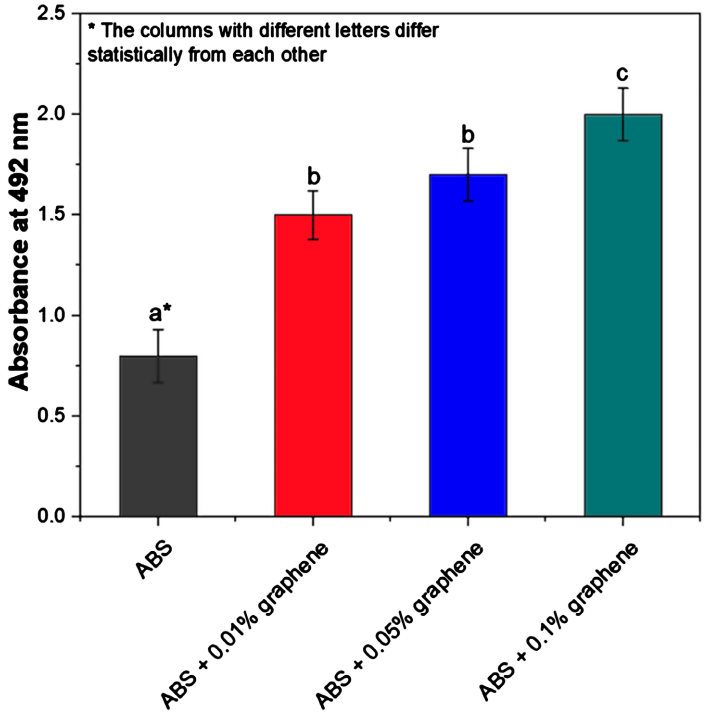

Figure 12. Absorbance of the neutral red dye absorption test of the surface adhered L929 cells.

to be captured. TGA and DSC indicate that the addition of graphene particles did not cause significant changes in the thermal structure of the material. Optical microscopy revealed large regions of clusters in the samples ABS-GNP 0.05% and ABS-GNP 0.1%, which can be observed on the surface of the material by the SEM technique. In turn, this is a crucial factor for the material effectiveness in cell viability and fixation. Finally, the material obtained was not cytotoxic and promoted cell adhesion above that presented by the pure polymer matrix.

The technology described in this article has the potential to serve as a basis for the development of future biocompatible materials that take advantage of their three-dimensional design to perform their functions.

Acknowledgements

The author would like to thank CAPES finance code 001, CNPQ and FAPERJ for the financial support of this work.

Conflicts of Interest

The authors declare no conflicts of interest regarding the publication of this paper.

References

[1] Huang, S.H., Liu, P., Mokasdar, A. and Hou, L. (2013) Additive Manufacturing and Its Societal Impact: A Literature Review. *The International Journal of Advanced Manufacturing Technology*, **67**, 1191-1203. https://doi.org/10.1007/s00170-012-4558-5

[2] Stansbury, J.W. and Idacavage, M.J. (2016) 3D Printing with Polymers: Challenges among Expanding Options and Opportunities. *Dental Materials*, **32**, 54-64. https://doi.org/10.1016/j.dental.2015.09.018

[3] Bodkhe, S., Turcot, G., Gosselin, F.P. and Therriault, D. (2017) One-Step Solvent Evaporation-Assisted 3D Printing of Piezoelectric PVDF Nanocomposite Structures. *ACS Applied Materials & Interfaces*, **9**, 20833-20842. https://doi.org/10.1021/acsami.7b04095

[4] Murphy, S.V. and Atala, A. (2014) 3D Bioprinting of Tissues and Organs. *Nature Biotechnology*, **32**, 773-785. https://doi.org/10.1038/nbt.2958

[5] Chizari, K., Arjmand, M., Liu, Z., Sundararaj, U. and Therriault, D. (2017) Three-Dimensional Printing of Highly Conductive Polymer Nanocomposites for EMI Shielding Applications. *Materials Today Communications*, **11**, 112-118. https://doi.org/10.1016/j.mtcomm.2017.02.006

[6] Farahani, R.D., Dubé, M. and Therriault, D. (2016) Three-Dimensional Printing of Multifunctional Nanocomposites: Manufacturing Techniques and Applications. *Advanced Materials*, **28**, 5794-5821. https://doi.org/10.1002/adma.201506215

[7] Dul, S., Fambri, L., Merlini, C., Barra, G.M.O., *et al.* (2017) Effect of Graphene Nanoplatelets Structure on the Properties of Acrylonitrile-Butadiene-Styrene Composites. *Polymer Composites*, **40**, E285-E300. https://doi.org/10.1002/pc.24645

[8] Almasi, N., Hosseinzadeh, S., Hatamie, S. and Sangsari, G.T. (2019) Stable Conductive and Biocompatible Scaffold Development Using Graphene Oxide (GO) Doped Polyaniline (PANi). *International Journal of Polymeric Materials and Polymeric Biomaterials*, **69**, 1-11. https://doi.org/10.1080/00914037.2019.1628028

[9] Ziąbka, M., Menaszek, E., Tarasiuk, J. and Wroński, S. (2018) Biocompatible Nanocomposite Implant with Silver Nanoparticles for Otology—*In Vivo* Evaluation. *Nanomaterials*, **8**, Article 764. https://doi.org/10.3390/nano8100764

[10] Rosenzweig, D., Carelli, E., Steffen, T., Jarzem, P. and Haglund, L. (2015) 3D-Printed ABS and PLA Scaffolds for Cartilage and Nucleus Pulposus Tissue Regeneration. *International Journal of Molecular Sciences*, **16**, 15118-15135. https://doi.org/10.3390/ijms160715118

[11] Farahani, R.D., Chizari, K. and Therriault, D. (2014) Three-Dimensional Printing of Freeform Helical Microstructures: A Review. *Nanoscale*, **21**, 10470-10485.

[12] Thingiverse.com (2015) Syringe Pump by Ameloot-Group. https://www.thingiverse.com/thing:819723

[13] Narayanamurthy, V., Samsuri, F., Firus Khan, A.Y., Hamzah, H.A., Baharom, M.B., Kumary, T.V., *et al.* (2019) Direct Cell Imprint Lithography in Superconductive Carbon black Polymer Composites: Process Optimization, Characterization and *in Vitro* Toxicity Analysis. *Bioinspiration & Biomimetics*, **15**, Article ID: 016002. https://doi.org/10.1088/1748-3190/ab1243

[14] ISO (2009) Biological Evaluation of Medical Devices—Part 5: Tests for *in vitro* Cytotoxicity. Comite Europeen de Normalisation.

[15] Zou, X.H., Foong, W.C., Cao, T., Bay, B.H., Ouyang, H.W. and Yip, G.W. (2004) Chondroitin Sulfate in Palatal Wound Healing. *Journal of Dental Research*, **83**, 880-885. https://doi.org/10.1177/154405910408301111

[16] Bokria, J.G. and Schlick, S. (2002) Spatial Effects in the Photodegradation of Poly (Acrylonitrile-Butadiene-Styrene): A Study by ATR-FTIR. *Polymer*, **43**, 3239-3246. https://doi.org/10.1016/S0032-3861(02)00152-0

[17] McCullough, E.J. and Yadavalli, V.K. (2013) Surface Modification of Fused Deposition Modeling ABS to Enable Rapid Prototyping of Biomedical Microdevices. *Journal of Materials Processing Technology*, **213**, 947-954. https://doi.org/10.1016/j.jmatprotec.2012.12.015

[18] (1964) Acetone. https://webbook.nist.gov/cgi/cbook.cgi?ID=C67641&Type=IR-SPEC&Index=2

[19] Cecci, R.R., Passos, A.A., Albino, N.R., Vicente, D.D., Duarte, A.S. and Tavares, M.I. (2020) Effect of Graphene Nanoplatelets Presence on the Thermal and Mechanical Properties of Polypropylene Fibers Produced by Melt Spinning. *Journal of Materials Science and Engineering B*, **10**, 53-63 https://doi.org/10.17265/2161-6221/2020.3-4.002